Weierstraß-Institut
für Angewandte Analysis und Stochastik

Leibniz-Institut im Forschungsverbund Berlin e. V.

Preprint ISSN 2198-5855

Synchronization between Kerr cavity solitons and broad laser pulse injection

Daria A. Dolinina, Andrei G. Vladimirov

submitted: November 18, 2024

Weierstrass Institute
Mohrenstr. 39
10117 Berlin
Germany
E-Mail: daria.dolinina@wias-berlin.de
andrei.vladimirov@wias-berlin.de

No. 3140
Berlin 2024

2020 *Mathematics Subject Classification.* 78A60, 35B32, 35C08, 34K40.

2010 *Physics and Astronomy Classification Scheme.* 42.65.-k, 42.65.Sf, 42.65.Pc, 42.65.Tg, 02.30.Ks.

Key words and phrases. Optical frequency comb, Kerr microcavity, synchronous pumping, cavity soliton, neutral delay differential equation.

The support by the Deutsche Forschungsgemeinschaft (DFG project No. 491234846) is gratefully acknowledged.

Edited by
Weierstraß-Institut für Angewandte Analysis und Stochastik (WIAS)
Leibniz-Institut im Forschungsverbund Berlin e. V.
Mohrenstraße 39
10117 Berlin
Germany

Fax: +49 30 20372-303
E-Mail: preprint@wias-berlin.de
World Wide Web: http://www.wias-berlin.de/

Synchronization between Kerr cavity solitons and broad laser pulse injection

Daria A. Dolinina, Andrei G. Vladimirov

Abstract

The synchronization of a soliton frequency comb in a Kerr cavity with pulsed laser injection is studied numerically. A neutral delay differential equation is used to model the light dynamics in the cavity. This model allows for the investigation of both cases where the pulse repetition period is close to the cavity round-trip time and where the repetition period of the injection pulses is close to a rational fraction M/N of the round-trip time. It is demonstrated that solitons can exist in this latter case, provided that the injection pulses are of a higher amplitude, which is directly proportional to the number M. Furthermore, it is shown that the synchronization range of the solitons is also proportional to the number M. The solitons excited by pulses with a period slightly different from the $M:N$-resonance can be destabilized by the Andronov-Hopf bifurcation, which occurs when the injection level at the soliton position decreases to M times the injection amplitude corresponding to the saddle-node bifurcation in a model equation with uniform injection.

The dynamics of solitons in Kerr microcavities has emerged as one of the central areas of research in nonlinear optics, driven by its profound implications for photonics and frequency comb technologies [1, 2]. Kerr microcavities, which exploit the Kerr nonlinearity to compensate the chromatic dispersion, enable the formation of the so-called temporal cavity solitons (TCS) - stable, self-reinforcing wave packets that propagate without changing shape [3, 4]. These solitons are critical to many applications ranging from high-precision metrology [5, 6] to telecommunications [7] and beyond [8, 9].

A novel approach to control soliton dynamics in optical microcavities is pulsed (synchronous) pumping [10]. Unlike continuous wave (CW) pumping, which maintains a constant energy input, pulsed injection is synchronized with the cavity round-trip time, introducing periodic energy perturbations and requiring much less energy to excite the TCS. This technique significantly affects soliton formation, their temporal position, stability, and bifurcations, resulting in diverse and complex dynamic behavior [11, 12, 13]. Pulsed injection has been shown to facilitate the generation of single solitons, soliton crystals, and chaotic states, expanding the toolkit for manipulating light in microcavities.

A standard method for modeling an optical microcavity with synchronous pumping is based on the application of the Lugiato-Lefever equation (LLE) [14]. The aforementioned approach was recently employed to demonstrate that in the absence of frequency mismatch between the repetition rate of the broad injection pulses and the inverse cavity round trip time, the stationary TCS is located at the top of the pulse when the pulse peak intensity is less than a specific pitchfork bifurcation threshold and is shifted to a position on the pulse periphery above this threshold [11, 12, 13, 15]. The introduction of frequency mismatch results in the stationary soliton position being determined by balancing the drift introduced by the mismatch with that due to the injection gradient. In order to describe the TCS motion in the presence of frequency mismatch and injection gradient, the soliton drift equation was proposed [16, 17], which is valid when the limit of small frequency mismatch and gradient is applicable. Nevertheless, the drift equation is insufficient for describing the bifurcation mechanism of TCS desynchronization as a function of increasing mismatch. As demonstrated in Ref. [18] the desynchronization of the system occurs via an Andronov-Hopf bifurcation when the repetition rate of the broad

DOI 10.20347/WIAS.PREPRINT.3140 Berlin 2024

injection pulse is close to the cavity round trip time. This phenomenon typically precedes the saddle-node bifurcation predicted by the drift equation and occurs when the injection level at the TCS position is reduced to the value corresponding to the saddle-node bifurcation in the LLE with CW injection.

Although the LLE approach is widely used for the analysis of soliton dynamics in optical microcavities, this approach is not free from certain limitations. In particular, it is not applicable to the study of TCS synchronization when the injection pulse repetition period is close to a multiple of the cavity round-trip times. Therefore, here we use an alternative model of an optical microcavity based on the neutral delay differential equation (NDDE) [19]. In contrast to the LLE, this model incorporates a sole independent time variable and is applicable to any ratio $M : N$ of cavity round-trip frequency and pulse repetition rate. In this study, we employ the NDDE model to investigate the impact of injection frequency detuning on TCS dynamics, with a particular focus on scenarios where the ratio $M : N$ approaches a rational number, with integer M and N. Our findings indicate that, akin to $1 : 1$ case, the TCS solutions can be exited with arbitrary M and N, although this process may necessitate much higher injection pulse peak powers. Starting from the NDDE model we derive an analog of the drift equation describing the slow time evolution of the soliton position and investigate how the synchronization range depends on the $M : N$ ratio.

1 Model equation

The NDDE model of a Kerr cavity can be represented in the following form [19]:

$$\left(A + \epsilon a \partial_t A + \epsilon^2 \frac{a^2 - ib}{2} \partial_{tt} A\right) e^{-i\epsilon^2 \alpha |A|^2/2 - i\epsilon^2 \theta/2} =$$
$$e^{-\epsilon^2} \left(A_\tau - \epsilon a \partial_t A_\tau + \epsilon^2 \frac{a^2 + ib}{2} \partial_{tt} A_\tau\right) e^{i\epsilon^2 \alpha |A_\tau|^2/2 + i\epsilon^2 \theta/2} + \epsilon^2 \eta(t), \tag{1}$$

where $A(t)$ is the complex field envelope and t is the time variable, $A_\tau = A(t - \tau)$, where τ is the cold cavity round-trip time. The coefficients a and b are the first- and second-order dispersion coefficients, respectively, α is the Kerr coefficient, θ is the detuning between the injection frequency and the frequency of a cavity mode, $\eta(t)$ is the laser injection term and ϵ describes small round-trip cavity losses. In the limit $\epsilon \to 0$ the NDDE model Eq. (1) can be reduced to the LLE [19]. Furthermore, it can be easily generalized to account for higher order dispersion terms by including higher order derivatives. We consider the injection in the form of pulses

$$\eta(t) = p \sin^{2k(1+ic)} \left(\frac{\pi}{T_{inj}} t\right). \tag{2}$$

where p is the amplitude of the pulses, T_{inj} is the repetition period of the injection pulses, integer k defines the width of the pulses and the term c defines the chirp of the pulse. In the following, the width of the injection pulse is selected in a manner that ensures it is smaller than the cavity round trip time and significantly larger than the TCS width.

As shown in [19] the equation (1) can exhibit stable TCS solutions under uniform pumping $\eta(t) = p_u$. In the mean-field limit, $\epsilon \to 0$, these TCSs coincide with those of the LLE. Unlike the LLE, where the TCS period is fixed by the periodic boundary condition, in the NDDE model the TCS repetition period depends on the parameters of Eq. (1). This period slightly exceeds the delay time τ and can be estimated as $T_s \approx \tau + 2\epsilon a + \mathcal{O}(\epsilon^2)$. Synchronization of the TCS with the external pulsed injection can take place when the repetition rate of injection pulses becomes close to one of the resonances,

in other words when $\frac{1}{T_s} : \frac{1}{T_{inj}} \equiv T_{inj} : T_s \approx M : N$ with integers M and N. In this context, the $M : N$ notation is employed to denote the corresponding resonances under consideration. Fig. 1 shows the TCS synchronization when $M : N = 8 : 1$ as an example. One can see that the solution train is T_{inj}-periodic and TCSs repeat themselves $M = 8$ round trips in the cavity. It can be seen from Fig. 1(c) that the TCS power decreases due to the cavity losses during the cavity round-trips between the injection pulses, where the intensity of these pulses is very small. The calculation of Fig. 1(a) involved a greater loss parameter than that used for Fig. 1(b). Consequently, the reduction in TCS power between the injection pulses is more pronounced in the former figure. The panel (c) demonstrates the spectra of the TCS from the panel (a) and the injection pulses.

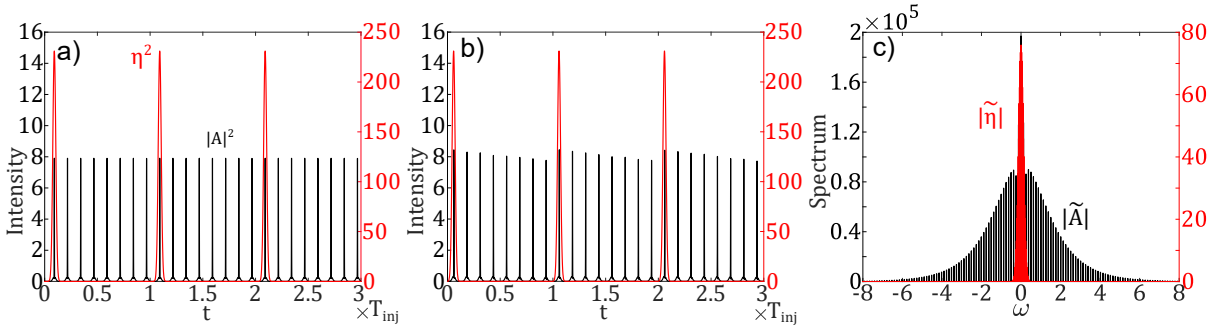

Figure 1: Solitons locked by the injection pulses with $T_{inj} \approx 8T_s$ in cases $\epsilon = 0.1$ (a) and $\epsilon = 0.01$ (b). Black and red lines with the corresponding axes show TCS intensity $|A|^2$ and injection intensity η^2, respectively. The spectrum of TCS and injection pulses from (a) panel (c). $\tilde{A}(\omega)$ and $\tilde{\eta}(\omega)$ are the Fourier transforms of $A(t)$ and $\eta(t)$ respectively. Cavity parameters are: $a = b = \alpha = \kappa = 1$, $\theta = -3.5$, and $\tau = 50$. Injection pulse parameters: $c = 0$, $p = 8p_u$, and $k = 128$, where $p_u = 1.9$ and $T_s \approx 50.02$ are the injection level and soliton period in the CW-pumped NDDE.

2 Numerical results

Let us start our analysis with the pulse period close to the resonance $1 : 1$. The synchronization of the TCS with the pulsed pumping means that the soliton period becomes equal to the injection pulse period T_{inj}, so we look for the periodic solution of (1) with period T_{inj}. To find such solutions we solve the boundary value problem with the periodic condition $A(0) = A(T_{inj})$ using the package DDE-BIFTOOL [20], which contains MATLAB routines for numerical bifurcation analysis of systems of delay differential equations. As an initial guess, the TCS solution under uniform pumping A_u with the period T_s is taken which converges to the final solution by Newton's iterations. The continuation of the TSC solution along the period T_{inj} is then performed with the DDE-BIFTOOL, which uses the pseudo-arclength method for continuation along the chosen parameter.

The branch of TCSs synchronized with the injection pulses of period close to the resonance $1 : 1$ and amplitude $p = p_u$ is shown by the yellow line in Fig. 2(a). The horizontal axis shows the period mismatch $\Delta = T_{inj} - T_s$ in dimensionless units of time. To recalculate them in dimensional time it is necessary to use a relation $\Delta' = \frac{nL}{c\tau}\Delta$, where n is the refractive index, L is the length of the resonator, c is the speed of light and τ is the dimensionless cold cavity round-trip time. It can be observed that the TCS peak intensity is maximal when the two periods coincide, $\Delta \approx 0$. The reason for this is the injection gradient which pushes the soliton towards the center of the pulse, where the

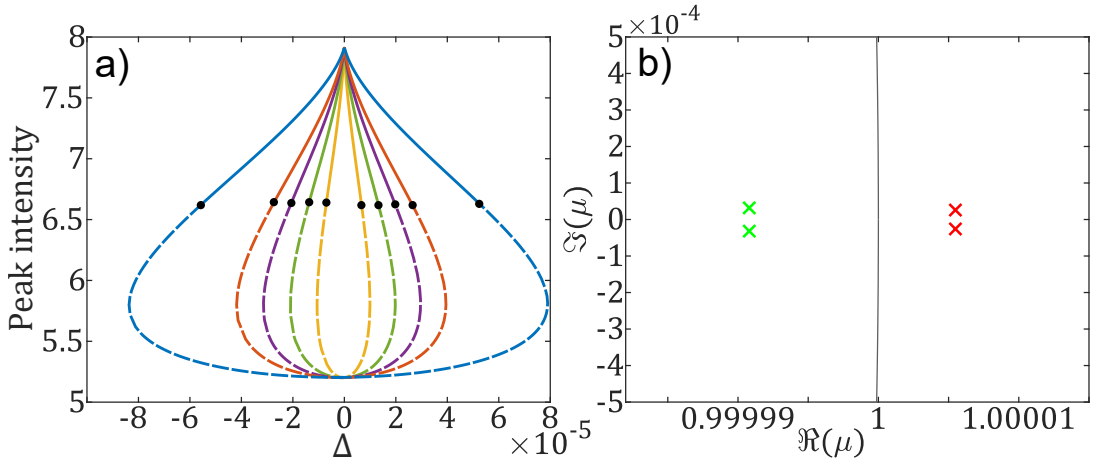

Figure 2: Soliton peak intensity as a function of $\Delta = NT_{inj} - MT_s$ for $M : N$ resonances, where $N = 1$ and $M = 1, 2, 3, 4, 8$, are shown by yellow, green, purple, red, and blue lines, respectively (a). Floquet multipliers responsible for soliton destabilization before (green crosses) and after (red crosses) the Andronov-Hopf bifurcation point for $M = 1$ (b). $\epsilon = 0.01$, other cavity parameters are the same as in Fig. 1. Injection pulse parameters: $c = 0$, $p = Mp_u$, $T_{inj} = (MT_s + \Delta)/N$ and $k = 2M^2$ for $M = 1, 2, 3, 4, 8$ respectively, where $p_u = 1.9$ and $T_s \approx 50.02$. Solid (dashed) lines indicate stable (unstable) solutions. Black dots show Andronov-Hopf bifurcation points.

amplitude of the injection is at its maximum [11, 12, 13]. Strictly speaking, the maximal peak intensity is slightly shifted from $\Delta = 0$. The discrepancy is due to the slight discrepancy between the TCS period and the calculated value of T_s. The latter was determined using a constant injection rate of $\eta = p$, which did not take into account the non-zero curvature of the injection at the top of the injection pulse. Given that the injection pulse is significantly broader than the TCS, the resulting change in period is negligible. A non-zero value of Δ results in the TCS drifting away from the top of the injection pulse. This leads to a decrease in the TCS peak power. Depending on the sign of Δ the soliton either lags or leads the pulse with each cavity round-trip. The drift can be compensated by means of injection gradient locking the TCS position. However, if the drift caused by Δ is too large, there is no periodic TCS solution. Therefore, the branch of solutions is limited by minimum and maximum values of Δ corresponding to saddle-node bifurcations. One can see that the branch of periodic TCS solutions is slightly asymmetric with respect to $\Delta \to -\Delta$ ($|\min(\Delta)| > |\max(\Delta)|$). This asymmetry is a consequence of the slight asymmetry inherent to the NDDE solitons. As the mean-field limit is approached, where the parameter ϵ tends to zero, the asymmetry diminishes. Conversely, as ϵ increases, the asymmetry becomes more pronounced.

In order to examine the stability of the synchronized T_{inj}-periodic solutions and to conduct an asymptotic analysis of the TCS motion, it is helpful to reformulate Equation (1) as a system of delay algebraic-differential equations:

$$\begin{aligned}
\partial_t A &= B \\
\partial_t B &= C \\
0 &= \left(A + \epsilon a B + \epsilon^2 \frac{a^2 - ib}{2} C\right) e^{-i\epsilon^2\alpha|A|^2/2 - i\epsilon^2\theta/2} - \\
&e^{-\epsilon^2\kappa} \left(B_\tau - \epsilon a B_\tau + \epsilon^2 \frac{a^2 + ib}{2} C_\tau\right) e^{i\epsilon^2\alpha|A_\tau|^2/2 + i\epsilon^2\theta/2} - \epsilon^2\eta(t),
\end{aligned} \tag{3}$$

The system can be reformulated in a more general form, as follows:

$$\mathcal{W}\partial_t\vec{X} = \vec{F}(\vec{X}, \vec{X}_\tau, \eta(t), \epsilon), \tag{4}$$

where $\mathcal{W}$ is 3×3 diagonal matrix with the diagonal elements $(1, 1, 0)$, $\vec{X} = (A, B, C)^T$, and $\vec{X}_\tau = (A_\tau, B_\tau, C_\tau)^T$.

To determine the stability of the synchronized TCS solution $\vec{X}_0(t) = \vec{X}_0(t+T_{inj})$ one must substitute a perturbed solution $\vec{X}(t) = \vec{X}_0(t)+\vec{\phi}(t)$ into Eq. (3) and linearize this equation around $\vec{X}_0(t)$. Then the resulting linear equation for the small perturbation $\vec{\phi}$ is:

$$\mathcal{W}\partial_t\vec{\phi}(t) = \mathcal{L}(t)\vec{\phi}(t) + \mathcal{M}(t)\vec{\phi}(t-\tau), \tag{5}$$

where $\mathcal{L}(t) = \partial_{\vec{X}}\vec{F}$ and $\mathcal{M}(t) = \partial_{\vec{X}_\tau}\vec{F}$ are T_{inj}-periodic Jacobian matrices with respect to $\vec{X}$ and $\vec{X}_\tau$. In accordance with Floquet theory, the solutions $\vec{\phi}(t)$ of the T_{inj}-periodic system (5), which satisfy the relation $\vec{\phi}(t+T_{inj}) = \mu\vec{\phi}(t)$, are the eigenfunctions and μ are the corresponding complex multipliers. Floquet multipliers are essential for characterizing the stability of the solution $\vec{X}_0$. If the absolute value of the Floquet multiplier, $|\mu|$, is not greater than one, the perturbation, $\vec{\phi}(t)$, will not grow with time. In the case of the uniform injection $\eta(t) = p_u = const$, Eq. (1) exhibits the time shift symmetry and the linear stability of the TCS necessitates that, with the exception of the neutral multiplier $\mu = 1$, which corresponds to this symmetry, all the absolute values of the Floquet multipliers remain below one. The nonuniform injection breaks the time-shift symmetry and eliminates the neutral multiplier from the TCS spectrum.

In Fig. 2(a) the stable (unstable) TCS solutions are represented by solid (dashed) curves. As can be observed, an increase (decrease) in Δ leads to a destabilization of the TCS before reaching the maximum (minimum) value of Δ corresponding to a saddle-node bifurcation. An examination of the Floquet multipliers reveals that the destabilization is due to an Andronov-Hopf bifurcation when two complex conjugate multipliers cross the unit circle $|\mu| = 1$, as shown in Fig. 2(b). This result is similar to that obtained using the LLE model in Ref. [18].

The main advantage of the NDDE model (1) over the LLE is that it is applicable in the case where the soliton is not pumped on every round-trip. In Fig. 2(a) different branches of synchronized TCS solutions correspond to the situation when the injection pulse arrives every Mth round-trip with $M = 1, 2, 3, 4, 8$ and is close to $M : 1$ resonances. To maintain an approximately constant pulse width for varying integer values of M and N, the power k in Eq. (2) was chosen so that the coefficient $\pi^2 k/T_{inj}^2$ in the second term of the Taylor expansion $\sin^{2k}(\pi t/T_{inj}) \approx 1-\pi^2 k\zeta^2/T_{inj}^2$ at $\zeta = t-T_{inj}/2 = 0$ was independent of M and N. Consequently, for $T_{inj} \approx M/NT_s$, we choose $k = 2M^2/N^2$ so that the injection stays at small ζ of the form $|\eta(\zeta)| \approx p\,(1 - 2\pi^2\zeta^2/T_s^2)$ with $T_s \approx 50.02$. As one can see in Fig. 2(a) the TCS can be synchronized to the injection pulse even with $M > 1$. It follows from this figure that to excite TCSs with approximately the same peak power as that obtained with $p = p_u$ and $M = 1$ using injection pulses with larger repetition periods $T_{inj} \approx MT_s$ $(M > 1)$, the amplitude of the injection pulses should be M times larger, $p = Mp_u$. It is seen that all the curves for different M and $p = Mp_u$ are similar and look like a scaling of the curve for $M = 1$. Note that we consider only the periodic solutions in the vicinity of the $M : N$ resonances with moderate M, which are the most interesting from a practical point of view. The complex dynamical regimes beyond the synchronization region are left for future investigation.

To gain insight into the rationale behind proportionally increasing the injection amplitude relative to the period T_{inj} to achieve a TCS with equivalent peak power, we examine the case of $M = 2$. The asymptotic approach is applied in a manner analogous to that utilized in deriving the LLE from the

NDDE model, as detailed in reference [19] (see also Ref. [21]). Let us assume that the TCSs are synchronized to the injection pulses with a period $T_{inj} \approx 2T_s$. Furthermore, let the detuning from the resonance $2:1$ be zero, which means that every second TCS sits on top of an injection pulse. In accordance with the aforementioned approach, we may express a stationary TCS solution to Eq. (1) in the form $A(t) = A_0(t_0) + \epsilon A_1(t_0) + \epsilon^2 A_2(t_0) + \mathcal{O}(\epsilon^3)$, where $t_0 = \omega t$ with $\omega = 1 - 2\epsilon a/\tau + (2\epsilon a/\tau)^2 + \mathcal{O}(\epsilon^3)$. These expansions are then substituted into Eq. (1) and the resulting terms are collected according to their respective powers of the variable ϵ. In zero order of the parameter ϵ, the solution is found to be τ-periodic $A_0(t_0) = A_0(t_0 - \tau)$. The first-order terms are collected, yielding the result that $A_1(t_0) = A_1(t_0 - \tau)$. In the second order of the parameter ϵ, the result is

$$A_2(t_0) - A_2(t_0 - \tau) = \tilde{\eta}\,(t_0) - (1 - i\theta)A_0(t_0) + i\alpha|A_0(t_0)|^2 A_0(t_0) + ib\partial_{t_0 t_0} A_0(t_0) \quad (6)$$

with $\tilde{\eta}\,(t_0) = \eta\,(t)$. In the case of uniform injection $\tilde{\eta}(t_0) = const$ all TCSs are identical and have the period T_s in the variable t corresponding to the period τ in the variable t_0. Hence $A_2(t_0)$ is also τ-periodic, the left-hand side of Eq. (6) is zero, and the amplitude A_0 satisfies the stationary LLE obtained by equating the right-hand side of Eq. (6) to zero. However, when the injection period becomes twice as large as T_s, the repetition period of the TCS also increases twice. Similarly, the second order correction period A_2 also becomes twice larger, $A_2(t_0) = A_2(t_0 - 2\tau)$. Let the time moment $t_0 = t_s$ correspond to the peak of the amplitude A_0 sitting on the top of the injection pulse. If we set $t_0 = t_s$ and $t_0 = t_s - \tau$ in Eq. (6) we obtain:

$$A_2(t_s) - A_2(t_s - \tau) = \eta_1 - (1 - i\theta)A_0(t_s) + i\alpha|A_0(t_s)|^2 A_0(t_s) + ib\partial_{t_0 t_0} A_0(t_s), \quad (7)$$

$$A_2(t_s - \tau) - A_2(t_s - 2\tau) = \eta_2 - (1 - i\theta)A_0(t_s) + i\alpha|A_0(t_s)|^2 A_0(t_s) + ib\partial_{t_0 t_0} A_0(t_s), \quad (8)$$

where $\eta_1 = \tilde{\eta}(t_s) = p$ is the amplitude of the injection pulse, $\eta_2 = \tilde{\eta}\,(t_s - \tau)$, and $A_0(t_s) = A_0(t_s - \tau)$ due to the τ-periodicity of A_0. Summing up Eqs. (7) and (8), dividing the result by 2, using 2τ periodicity of A_2, and taking into account that the injection is present only on one cavity round-trip from two, $\eta_2 = 0$, we get

$$\frac{p}{2} - (1 - i\theta)A_0(t_s) + i\alpha|A_0(t_s)|^2 A_0(t_s) + ib\partial_{t_0 t_0} A_0(t_s) = 0,$$

It follows from this equation that in order to obtain the same TCS peak amplitude $A_0(t_s)$ using one pulse per two cavity round-trips, one needs twice the injection pulse amplitude p as in the case of one pulse per one cavity round-trip. Note that this property holds in the mean field limit, $\epsilon \to 0$, and assumes that the injection pulse is much wider than the TCS so that the injection is approximately constant across the soliton. With the deviation from the $\epsilon \to 0$ limit the TCS intensity decays on every round-trip between the injection pulses. Fig. 1 demonstrates how TCSs change between the injection pulses for $\epsilon = 0.1$ in panel (a) and for $\epsilon = 0.01$ in panel (b) when the TCS is pumped every 8th round-trip. The figure shows that the TCS peak intensity stays almost the same for $\epsilon = 0.01$ and changes more noticeably at higher $\epsilon = 0.1$.

3 Asymptotic drift equation

As was shown in previous works [11, 12] for zero period mismatch the stationary position of the synchronized TCS is at the centre of the injection pulse (if $p < p_c$, where p_c is the value of the injection amplitude at which pitchfork bifurcation occurs). A small period mismatch shifts the stationary TCS position away from the centre of the pulse and such a shift results in a decrease of the soliton intensity. The drift equation for determining the TCS position relative to the injection pulse, based on

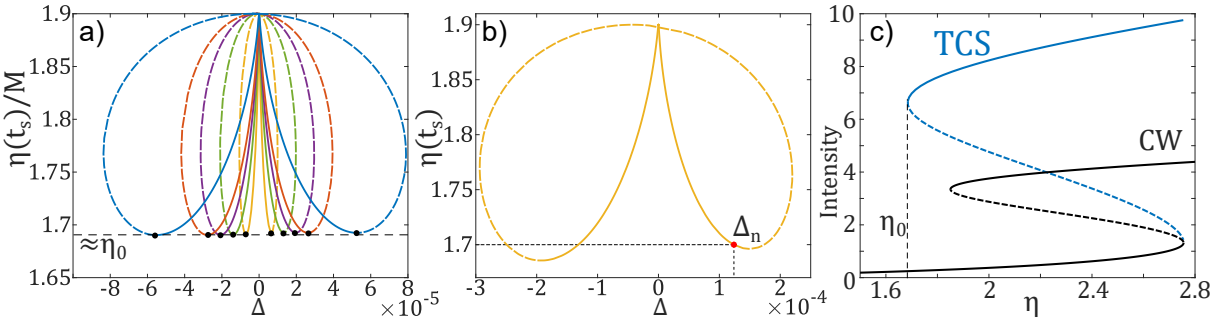

Figure 3: Injection amplitude $\eta(t_s)$ at the soliton position t_s as a function of the period mismatch Δ for the parameters from Fig.2(a) (a). Same as in (a), but only for $1:1$ resonance and for $\epsilon = 0.05$ (b). CW and peak TCS intensity dependence on the amplitude of the uniform injection $\eta = p_u$ (c).

the given period mismatch, was derived for the LLE model in [12]. An analogous equation can be derived for the NDDE model. To obtain such an equation we use a perturbative approach and look for the solution of the Eq. (3) in the form $\vec{X}(t) = \vec{X}_0(\xi)$, where $\xi = t + t_s(t) - Vt$. Here, t_s is a slowly varying TCS coordinate, $\partial_t t_s = \mathcal{O}(\delta)$, $V = \mathcal{O}(\delta)$ is the small drift velocity due to the frequency mismatch, and $\vec{X}_0(t)$ is the TCS solution of Eqs. (3) under uniform pumping $\eta = p_u$, corresponding to the injection value at the soliton position $p_u = \eta(t_s)/M$. The drift velocity can be expressed as $V = N - \dfrac{MT_s}{T_{inj}}$. Then, similarly to [12] we expand the injection in the soliton position t_s and assume that the injection gradient $\eta'_{t_s} = \partial_t \eta|_{t=t_s}$ is of order of δ, while the constant injection term equals p_u. As a result, in the first order of δ, we obtain a TCS drift equation similar to that reported in [11, 12]:

$$\frac{dt_s}{dt} = V + \epsilon^2 \eta'_{t_s} \frac{\left\langle \vec{\psi}^\dagger \middle| \vec{w}\xi \right\rangle}{\left\langle \vec{\psi}^\dagger \middle| \mathcal{W}\vec{\psi} \right\rangle}, \tag{9}$$

where $\vec{\psi} = \partial_t \vec{X}$ is the column vector neutral mode associated with the time translation symmetry of Eqs. (1) and (3) with uniform injection p_u. This mode is the T_s-periodic solution of the linear equation (5) and corresponds to the Floquet multiplier $\mu = 1$. The adjoint neutral mode $\vec{\psi}^\dagger$ is the T_s-periodic row vector solution of the equation $\partial_t \vec{s}^\dagger(t)\mathcal{W} = \vec{s}^\dagger(t)\mathcal{L}(t) + \vec{s}^\dagger(t+\tau)\mathcal{M}(t+\tau)$ adjoint to Eq. (5) [22]. Since only the third equation in the system (3) contains the perturbed injection term, the first two components of the vector $\vec{w}$ are equal to zero, $\vec{w} = (0, 0, 1)^T$. The stationary TCS solution exists when the right-hand side of Eq. (9) equals zero. Therefore, the maximum and minimum values of the frequency mismatch parameter V, which can be compensated by the last term in Eq. (9), define the range of stationary TCS existence.

As mentioned before, in our calculations the shape of the injection pulse remains approximately the same for different M, and only the injection amplitude is changed proportionally to its period, $|\eta(\zeta)| \approx M p_u \left(1 - \dfrac{2\pi^2\zeta^2}{T_s^2}\right)$. Hence, the gradient term in Eq. (9) is also directly proportional to the injection pulse amplitude Mp_u. From this we can conclude that the width of the interval in V (and correspondingly in Δ) where the TCS solution exists is also proportional to M. This can be clearly seen in Fig. 2(a), where the curves computed with $M > 1$ look like the scaled in M versions of the curve for $M = 1$. Furthermore, the points of TCS destabilization through an Andronov-Hopf bifurcation are also scaled by M, although the local injection value $\eta(t_s)/M$ remains the same, see Fig. 3(a,b). This value corresponds to the saddle-node bifurcation injection value in the uniform case $\eta(t_s)/M \approx \eta_0$, shown in Fig. 3(c). Such a result is in good agreement with Ref. [18], where this phenomenon was

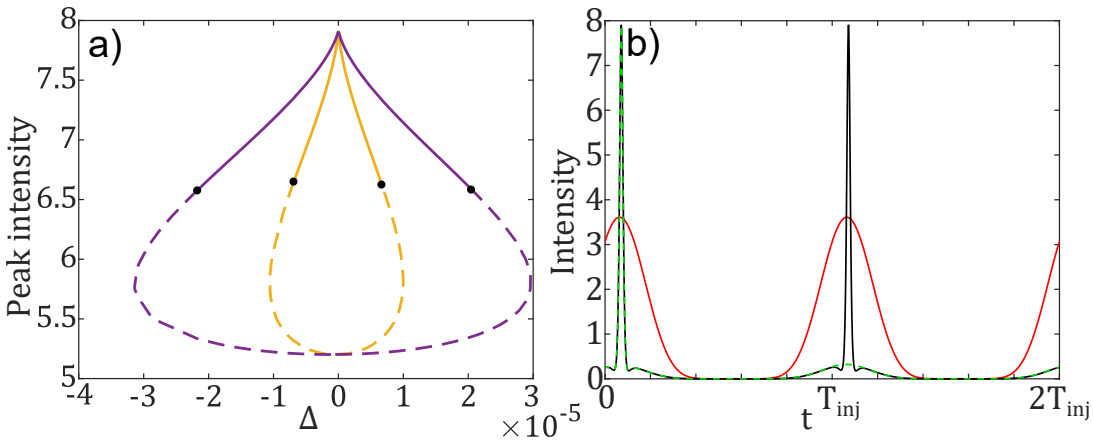

Figure 4: Soliton peak intensity as a function of Δ for $1:2$ $(3:2)$ shown by yellow (purple) color (a). Two possible periodic states with one (green dashed line) or two (black solid line) solitons excited by the injection pulses with $T_{inj} = T_s/2$ (b). $\tau = 100$ and $T_s \approx 100.02$, other cavity and injection pulse parameters are the same as in Fig. 2.

demonstrated and discussed for the LLE model.

Let us evaluate the quantitative accuracy of the predictions provided by Eq. (9). For this, we need to compare the value Δ_n calculated numerically with the analytically predicted value $\Delta_a = VT_{inj} = -\epsilon^2\eta'_{t_s}\dfrac{\left\langle\vec{\psi}^\dagger\middle|\vec{w}\xi\right\rangle}{\left\langle\vec{\psi}^\dagger\middle|\mathcal{W}\vec{\psi}\right\rangle}T_{inj}$. As an example, we calculate Δ_n and Δ_a for the injection value $\eta(t_s) = 1.7$ corresponding to the red dot in Fig. 3(b). First, we need to compute the neutral $\vec{\psi}$ and adjoint neutral $\vec{\psi}^\dagger$ modes for the uniform injection case with $\eta(t) = p_u = 1.7$. To unambiguously define the adjoint mode $\psi^\dagger$, the DAE system (3) was reformulated as a delay differential equation (DDE) system by introducing Lorentzian spectral filter of width d^{-1} into the cavity, as described in [19]. The resulting system of DDEs (Eq. (32) in Ref.[19]) converges to the original system (3) in the limit $d \to 0$. Thus, the adjoint neutral mode $\vec{\psi}^\dagger$ is calculated from the DDE system in this limit. The values of the position t_s and the injection gradient η'_{t_s} are obtained from the shape of the injection pulse (2) for a given p_u. Calculating all modes and values for the parameters of Fig. 3(b) with $p_u = 1.7$ we get $\Delta_a \approx 1.143 \times 10^{-4}$, while the result of the numerical calculation is $\Delta_n \approx 1.239 \times 10^{-4}$. So the results differ by less than 10%.

Let us now consider the case $N > 1$, corresponding to the situation where there are N injection pulses in M cavity round trips. In the case of $1:2$ resonance, the injection period is $T_{inj} \approx 1/2T_s$, so there are two injection pulses per period T_s. Two injection pulses can either excite two solitons or alternatively generate a single soliton, as shown in Fig. 4(b). These two scenarios correspond to the TCS solution branches that coincide with the graphical precision when plotted in Δ peak intensity coordinates. These branches are represented by the yellow line in Fig. 4(a). This figure was calculated with the same shape and amplitude of the injection pulse as Fig. 2(a). A comparison of the yellow branches for resonances $1:2$ in Fig. 4 and $1:1$ in Fig. 2(a) reveals a striking similarity, with both branches closely coinciding. This observation can be easily confirmed using the drift equation (9), which shows that the maximum value of V corresponding to a saddle-node bifurcation remains unchanged over $1:N$ resonances for any integer N. Moreover, the same result holds for any fixed value of M. In particular, the branch for the $3:2$ resonance shown by the purple line in Fig. 4 is similar to the one corresponding to the $3:1$ resonance in Fig. 2(a).

In the results discussed above, only injection pulses with amplitudes below the pitchfork bifurcation

threshold and without chirp are considered. However, it is important to emphasise that the synchronization range is proportional to M, regardless of the value of the pump amplitude and regardless of whether the pulses exhibit chirp or not. Figure 5(a) shows the solution branches for the case where the pulse amplitude p exceeds the pitchfork threshold p_c. Here, in contrast to the case $p < p_c$ where only a single stable TCS exists at $\Delta = 0$, there are three TCSs at zero period mismatch above the pitchfork bifurcation threshold, one unstable and two stable. The TCS branch calculated for the resonances $1:1$ and $2:1$ are proportional to each other. The same proportionality is preserved even when the injection pulse is chirped, see Fig. 5(b).

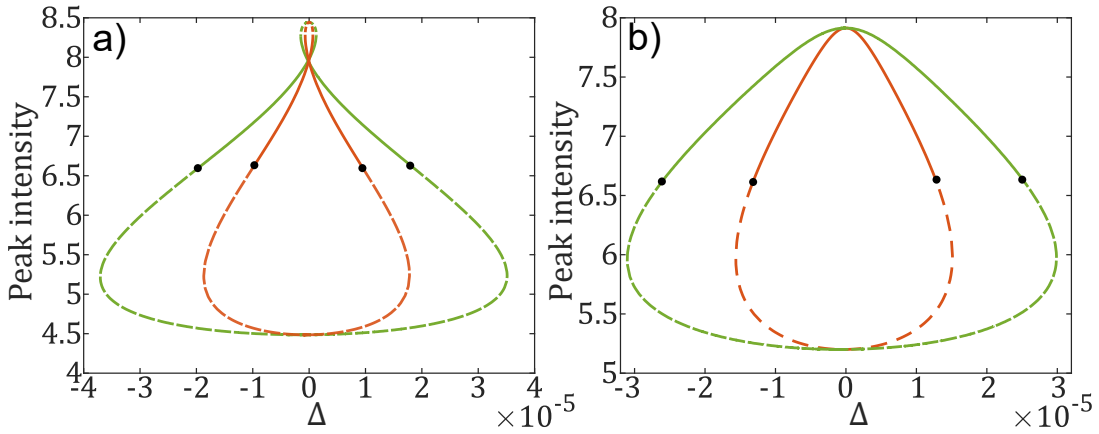

Figure 5: Soliton peak intensity as a function of Δ for the resonance $1:1$ $(2:1)$ shown by red (green) color for the case $p = 2.1 > p_c$ (a). Soliton peak intensity as a function of Δ for the resonance $1:1$ $(2:1)$ shown by red (green) color in the presence of chirp, $c = 0.5$ for $p = 1.9 < p_c$ (b). Other cavity and injection pulse parameters are the same as in Fig. 2.

4 Discussion

The synchronization of TCSs with pulsed laser injection in a Kerr cavity is considered using a neutral delay differential equation model. Although the numerical integration of this model is more time-consuming compared to a standard modelling approach based on the LLE, it allows us to study the more complex synchronization scenarios, in particular those where the soliton is not pumped on every round-trip. We show that if the TCS is pumped by injection every Mth round-trip, the amplitude of the injection pulses should be increased proportionally to the number M in order to excite a TCS with approximately the same peak power. This means that the intensity of each pulse is increased by a factor of M^2, while the repetition frequency is reduced by a factor of M compared to the case where a TCS is pumped on each round trip. On the other hand, the synchronization range is also increased by a factor of M. In other words, one would have to use M times more energy to get the TCS pumped every Mth round trip, but the synchronization region is also increased by a factor of M. Furthermore, our results indicate that the synchronization region exhibits a proportional increase with respect to M, independent of the corresponding injection pulse amplitude at $M = 1$ and the presence of the chirp.

We have derived an asymptotic drift equation similar to that previously reported for the LLE [11, 12, 17]. This equation predicts the stationary soliton saddle-node bifurcation when the mismatch between the

injection period and the TCS period is sufficiently large, but is not sufficient to estimate the TCS synchronization range, which is limited by Andronov-Hopf bifurcations [18]. We have shown that when the injection pulse period is close to M cavity round-trip times, this bifurcation occurs when the injection level at the TCS position drops to the value $M\eta_0$, where η_0 is the injection rate corresponding to the saddle-node bifurcation of the NDDE with homogeneous injection. In addition, we considered a scenario with multiple injection pulses during the cavity traversal time and showed that in this case the synchronization range remains unchanged regardless of whether each pulse generates a soliton or not.

References

[1] Alessia Pasquazi, Marco Peccianti, Luca Razzari, David J Moss, Stéphane Coen, Miro Erkintalo, Yanne K Chembo, Tobias Hansson, Stefan Wabnitz, Pascal Del'Haye, et al. Micro-combs: A novel generation of optical sources. *Physics Reports*, 729:1–81, 2018.

[2] Alexander L Gaeta, Michal Lipson, and Tobias J Kippenberg. Photonic-chip-based frequency combs. *Nature Photonics*, 13(3):158–169, 2019.

[3] T. Herr, V. Brasch, J. D. Jost, C. Y. Wang, N. M. Kondratiev, M. L. Gorodetsky, and T. J. Kippenberg. Temporal solitons in optical microresonators. *Nat. Photonics*, 8:145–152, 2014.

[4] Tobias Herr, Michael L Gorodetsky, and Tobias J Kippenberg. Dissipative kerr solitons in optical microresonators. *Nonlinear optical cavity dynamics: from microresonators to fiber lasers*, pages 129–162, 2016.

[5] Philipp Trocha, M Karpov, D Ganin, Martin HP Pfeiffer, Arne Kordts, S Wolf, J Krockenberger, Pablo Marin-Palomo, Claudius Weimann, Sebastian Randel, et al. Ultrafast optical ranging using microresonator soliton frequency combs. *Science*, 359(6378):887–891, 2018.

[6] Nathalie Picqué and Theodor W Hänsch. Frequency comb spectroscopy. *Nat. Photonics*, 13(3):146–157, 2019.

[7] Jochen Schröder, Attila Fülöp, Mikael Mazur, Lars Lundberg, Óskar B Helgason, Magnus Karlsson, Peter A Andrekson, et al. Laser frequency combs for coherent optical communications. *J. Light. Technol.*, 37(7):1663–1670, 2019.

[8] Tara Fortier and Esther Baumann. 20 years of developments in optical frequency comb technology and applications. *Commun. Phys.*, 2(1):1–16, 2019.

[9] Lin Chang, Songtao Liu, and John E Bowers. Integrated optical frequency comb technologies. *Nature Photonics*, 16(2):95–108, 2022.

[10] Ewelina Obrzud, Steve Lecomte, and Tobias Herr. Temporal solitons in microresonators driven by optical pulses. *Nature Photonics*, 11(9):600–607, 2017.

[11] Ian Hendry, Wei Chen, Yadong Wang, Bruno Garbin, Julien Javaloyes, Gian-Luca Oppo, Stéphane Coen, Stuart G Murdoch, and Miro Erkintalo. Spontaneous symmetry breaking and trapping of temporal Kerr cavity solitons by pulsed or amplitude-modulated driving fields. *Physical Review A*, 97(5):053834, 2018.

[12] Ian Hendry, Bruno Garbin, Stuart G Murdoch, Stéphane Coen, and Miro Erkintalo. Impact of desynchronization and drift on soliton-based Kerr frequency combs in the presence of pulsed driving fields. *Physical Review A*, 100(2):023829, 2019.

[13] Ian Hendry. *Novel dynamics of driven nonlinear resonators*. PhD thesis, ResearchSpace@ Auckland, 2020.

[14] Luigi A Lugiato and René Lefever. Spatial dissipative structures in passive optical systems. *Phys. Rev. Lett.*, 58(21):2209, 1987.

[15] Francesco Rinaldo Talenti, Yifan Sun, Pedro Parra-Rivas, Tobias Hansson, and Stefan Wabnitz. Control and stabilization of Kerr cavity solitons and breathers driven by chirped optical pulses. *Optics Communications*, 546:129773, 2023.

[16] T Maggipinto, M Brambilla, GK Harkness, and WJ Firth. Cavity solitons in semiconductor microresonators: Existence, stability, and dynamical properties. *Phys. Rev. E*, 62(6):8726, 2000.

[17] Miro Erkintalo, Stuart G Murdoch, and Stéphane Coen. Phase and intensity control of dissipative Kerr cavity solitons. *Journal of the Royal Society of New Zealand*, 52(2):149–167, 2022.

[18] D. A. Dolinina, G. Huyet, D. Turaev, and A. G. Vladimirov. Desynchronization of temporal solitons in kerr cavities with pulsed injection. *Opt. Lett.*, 49:4050–4053, 2024.

[19] Andrei G. Vladimirov and Daria A. Dolinina. Neutral delay differential equation model of an optically injected Kerr cavity. *Phys. Rev. E*, 109:024206, Feb 2024.

[20] K. Engelborghs, T. Luzyanina, and G. Samaey. DDE-BIFTOOL v.2.00: A MATLAB package for bifurcation analysis of delay differential equations. Technical Report TW-330, Department of Computer Science, K.U.Leuven, Leuven, Belgium, 2001.

[21] Theodore Kolokolnikov, Michel Nizette, Thomas Erneux, Nicolas Joly, and Serge Bielawski. The Q-switching instability in passively mode-locked lasers. *Phys. D: Nonlinear Phenom.*, 219(1):13–21, 2006.

[22] A. Halanay. *Differential Equations: Stability, Oscillations, Time Lags*. Academic Press: New York, NY, USA, 1966.